# Accurate optical measurement of nuclear polarization in optically pumped 3He gas

N. Bigelow, P. Nacher, M. Leduc

Classification
*Physics Abstracts*
32.80B — 42.60K — 67.65

# Accurate optical measurement of nuclear polarization in optically pumped $^3$He gas

N. P. Bigelow (*), P. J. Nacher and M. Leduc

Laboratoire de Spectroscopie Hertzienne (**), Ecole Normale Supérieure, 24 rue Lhomond, 75231 Paris, France

(*Received 10 June 1992, accepted in final form 8 September 1992*)

**Résumé.** — On peut maintenant produire par pompage optique de fortes polarisations nucléaires $M$ ($M$ supérieure à 80 %) dans l'$^3$He gazeux. Le gaz est excité par une décharge radiofréquence et orienté à l'aide d'un laser LNA de forte intensité qui est pompé par des lampes et accordé sur la transition 2 $^3$S-2 $^3$P à 1,08 μm. Dans cet article, nous décrivons une expérience où nous mesurons $M$ avec une grande précision absolue. Notre méthode est fondée sur la variation en fonction de $M$ de l'absorption par les atomes métastables d'un faisceau sonde de faible intensité polarisé linéairement. Nous mesurons le rapport des absorptions pour des polarisations $\pi$ et $\sigma$. Le faisceau sonde est un laser LNA pompé par diode qui se propage perpendiculairement à la direction de l'aimantation. Simultanément, nous mesurons $M$ par le degré de polarisation circulaire $\mathcal{P}$ de la raie à 668 nm émise par la décharge. Nos résultats montrent une relation linéaire entre $M$ et $\mathcal{P}$ dans toute la gamme des valeurs de $M$ réalisées et pour des conditions expérimentales variées (pression dans la cellule, champ magnétique, niveau de décharge, etc.). Ceci fournit une seconde méthode pour mesurer la polarisation nucléaire de l'$^3$He. Cette méthode est simple à mettre en œuvre et se trouve ainsi calibrée dans une gamme de pression allant de 0,15 à 6,5 torr.

**Abstract.** — Large nuclear polarizations $M$ (over 80 %) can now be achieved in gaseous $^3$He by optical pumping. The gas is excited by an RF discharge and is oriented using a high power LNA laser which is lamp pumped and tuned to the 2 $^3$S-2 $^3$P transition at 1.08 μm. In this paper we describe an experiment in which we measure $M$ with high absolute precision. Our method is based on a change as a function of $M$ in the ratio of $\sigma$ or $\pi$ polarized light absorbed from a weak probe beam by the 2 $^3$S metastable atoms. The probe was delivered by a diode pumped LNA laser and propagated perpendicular to the direction of the magnetization. Simultaneous measurement of $M$ was made by monitoring the degree of circular polarization $\mathcal{P}$ of the optical line at 668 nm emitted by the discharge. Our measurements show a linear relationship between $M$ and $\mathcal{P}$ for all accessible $M$ values and for a wide range of experimental conditions (sample pressure, magnetic field, RF discharge level, etc.). This provides a second method of measurement of the $^3$He nuclear polarization which is simple to operate and is calibrated over a pressure range of 0.15 to 6.5 torr.

(*) *Permanent Address :* Department of Physics and Astronomy and Laboratory for Laser Energetics, University of Rochester, Rochester, N.Y. 14627, U.S.A.

(**) Laboratoire associé au CNRS URA 18.

**Introduction.**

Optical pumping is an efficient method for creating nuclear polarization in a gas of $^3$He. Polarized $^3$He has applications in different fields of physics ranging from quantum fluids [1] to nuclear physics [2]. Optical pumping of $^3$He was first demonstrated in 1963 [3]. More recently there has been a renewed interest in this technique because of the increasingly high values of nuclear polarization $M$ which have been achieved. Much of the recent progress has resulted from the development of efficient solid state IR lasers capable of exciting the 2 $^3$S-2 $^3$P $^3$He transition at 1.08 μm. In particular, using a lamp pumped LNA laser which delivers a few watts of CW power [4-6], it is possible to achieve values of $M$ in excess of 80 %. As a direct result of these improvements in $M$ values, accurate techniques for measuring $M$ are increasingly in demand. For example, consider nuclear physics scattering experiments [7] which use polarized helium targets. In these experiments asymmetries are measured in scattering cross sections for reversal of target polarization and hence the experiments require that $M$ be both large and precisely known.

In general, one can distinguish several methods for measuring $M$ in optically pumped $^3$He. The first group relies on a direct magnetic measurement. Such a measurement can be made either by measuring the magnetic field created by the sample using an absolute magnetometer [8] or by magnetic resonance (NMR). NMR techniques were used in the early experiments [3] with pure $^3$He and also for $^3$He polarized by spin exchange with optically pumped rubidium vapor [9]. The $^3$He NMR signals must be calibrated against a known reference sample of identical geometry such as the proton reference provided by a sample cell of pure water. This method, already used in earlier experiments [3], is currently being examined with increased accuracy [10].

The second group of measurements is optical and relatively simple to operate as compared to magnetic measurements and the measurement apparatus can be more easily isolated from the polarized sample. $M$ is determined by analysis of the absorption of the 2 $^3S_1$ metastable atoms or of the polarization of the light emitted by the discharge. The absorption method has been demonstrated by several groups using He lamps as the probe source [3, 11, 12] and requires a model of the optical pumping process to extract absolute $M$ values. The analysis of the polarization distribution of the emission spectra was introduced by Laloë [13, 14]. This method relies on the conservation of nuclear spin during collisions which excite atoms from the ground state to an upper state ; in the excited state the hyperfine interaction couples the nuclear and electronic degrees of freedom such that the electronic polarization, and hence the polarization of the light emitted as the excited state decays through spontaneous emission, both reflect the state of nuclear polarization. This method provides a practical technique for monitoring $M$, but is too complex to directly provide absolute values for $M$, so it must be calibrated against an other method [15]. The precision of previous absorption measurements has been limited by the lack of detailed knowledge of the coincidence of the lamp profile with the atomic absorption spectrum. The same limitations arose in early studies of polarization distribution of the emitted light, because they were calibrated through absorption methods.

In the present work, we describe experiments in which $M$ is directly measured by absorption of a probe beam with a greatly increased absolute accuracy. The improvements are achieved by using a diode pumped tunable single-mode LNA laser to create the probe beam and by using a revised experimental geometry to eliminate sources of systematic error. We have used this absorption technique to recalibrate the $M$ dependence of the optical polarization distribution of one of the He emission lines (3 $^1$D-2 $^1$P at 668 nm), and to extend this calibration to high values of $M$.

Measurements were carried out under a large range of experimental conditions : discharge level, sample pressure, magnetic field and polarization rates were varied. In this article we first

discuss the principle of our polarization measurement *via* absorption. We then go on to describe the experimental set-up and measurement procedure, and finish the paper with a presentation of our results and a discussion of the estimated accuracies.

**1. Principle of polarization measurement used in this work.**

Absorption measurements were performed using a weak probe beam tuned to the $C_9$ transition of the $^3$He $\left(2\,^3S_1,\ F = \frac{3}{2} \rightarrow 2\,^3P_0,\ F = \frac{1}{2}\right)$ (see Fig. 1). The absorption $\mathcal{A}_p$ of the probe beam was measured as a function of its optical polarization $p$. In our experiments, as in the early work of reference [12], we measured the absorption for a linearly polarized probe. In the present experiment, the probe polarization had components both perpendicular ($p = \sigma$) and parallel ($p = \pi$) to the quantization axis. The two measured absorption signals are proportional to the metastable atom density, $n_m$ [1]; they also depend on the relative populations of the magnetic sublevels $\left(m_F = -\frac{3}{2}, \ldots, +\frac{3}{2}\right)$ of the $2\,^3S_1$, $F = \frac{3}{2}$ state and thus depend on the nuclear polarization of the metastable atoms. For example, when the $2\,^3S_1$,

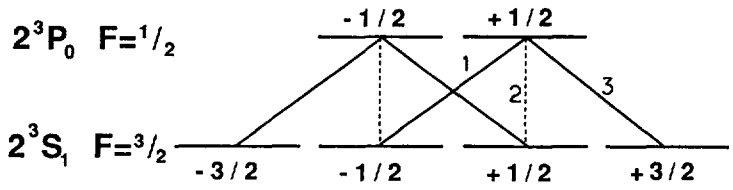


Fig. 1. — Magnetic sublevels involved in the optical detection using the $C_9$ component of the $^3$He transition ($2\,^3S_1,\ F = \frac{3}{2} \rightarrow 2\,^3P_0$). The solid lines are $\sigma$ transitions, the dotted lines are $\pi$ transitions. The numbers indicated along the transitions are the relative oscillator strengths.

$F = \frac{3}{2}$ state is fully polarized, only the $m_F = \frac{3}{2}$ state is populated, and by conservation of angular momentum (i.e. the angular momentum selection rules), if the probe beam is $\pi$ polarized, the absorption $\mathcal{A}_\pi \rightarrow 0$. In comparison, the absorption $\mathcal{A}_{\sigma^-}$ of a $\sigma^-$ polarized probe is enhanced as compared to the case where there is no net nuclear polarization ($M = 0$). To relate the measured values of absorption to the ground state polarization $M$, we use calculations of the $^3$He pumping process which explicitly treat the coupling of the polarization between different atomic levels involved and for which a generalized model was derived previously [16]. The key point is that the nuclear spin polarization of the ground state and of the $2\,^3S_1$ metastable state atoms are very strongly coupled by metastability exchange collisions. The model of reference [16] allows a direct calculation of the metastable atom populations under the joint influence of such exchange collisions, of the absorption of the pump laser and subsequent reemission, and of various relaxation phenomena. It introduces a parameter $n_m^*/n_m$ corresponding to the fraction of the metastable atoms directly interacting with the pump laser. Actually, in the present experiment, where the pump source is a lamp pumped

(1) This could become inaccurate if the total absorption in the cell were not small ; in such a situation an explicit calculation of each polarization component of the probe beam would be required. In most of our experimental situations the total attenuation was of order 1 % (up to 5 % at the highest) so that a linear approximation is adequate.

LNA laser (see Sect. 2.1), the fraction $n_m^*/n_m$ is a relatively large number [17], ranging between 0.1 and 1.0, because the mode structure of the laser is relatively broad, and hence a large range of atomic velocity classes absorb. Using the complete formalism of reference [16] it is thus possible to calculate exactly the probe absorption signals $\mathcal{A}_\pi$, $\mathcal{A}_{\sigma-}$ and $\mathcal{A}_{\sigma+}$ as a function of $M$ for given values of the parameters $n_m^*/n_m$ and $n_m$. The other input parameters of the calculation are the ground state density $N$, the nuclear relaxation time $T_1$ and the metastable relaxation time $\tau_r$. Note that the ratio $\mathcal{A}_\pi/\mathcal{A}_\sigma$ is independent of $n_m$.

All the experiments described in this work were performed in the absence of the pump beam (see Sect. 3.1). In this case a simplified version of the model can be used, given that the rate of metastability exchange collisions [18] ($\approx 10^6\ s^{-1}$) is much faster than the metastable relaxation rate ($\tau_r$ is on the order of the diffusion time across the cell, typically of order $10^{-3}$ s). As discussed in references [3] and [12], one can thus assume that the metastable and ground state atoms come, through collisions, into a « Boltzmann-type » distribution in angular momentum (instead of energy) in which the population $n(m)$ of the $m^{th}$ magnetic sublevel of the $2\ ^3S_1$ state is given by $n(m) \sim e^{-\beta m}$ where $\beta$ is a constant. The value for $\beta^{-1}$ (the effective « spin temperature ») for the ground state is the same as for the metastable state. The differences between the results of this simplified model and those of the more complete model of reference [16] are discussed in appendix 1. The error introduced by using the simplified model are less than 0.1 % for pressures greater than 0.7 torr. For lower pressures a small correction is evaluated in appendix 1 and quoted in the table I which is displayed in section 3.3.

The predictions for the absorption signals calculated with this simplified model are shown in figure 2a. It shows the normalized absorptions $\mathcal{A}_{\sigma+}$, $\mathcal{A}_{\sigma-}$ and $\mathcal{A}_\pi$ as a function of nuclear polarization $M$. The figure also shows the absorption $\mathcal{A}_\sigma$ for a beam carrying equal intensities of $\sigma_+$ and $\sigma_-$ polarized light. The vertical scale is proportional to the metastable atom density. For small $M$ values the absorptions $\mathcal{A}_\sigma$ and $\mathcal{A}_\pi$ are relatively insensitive to $M$. As pointed out in

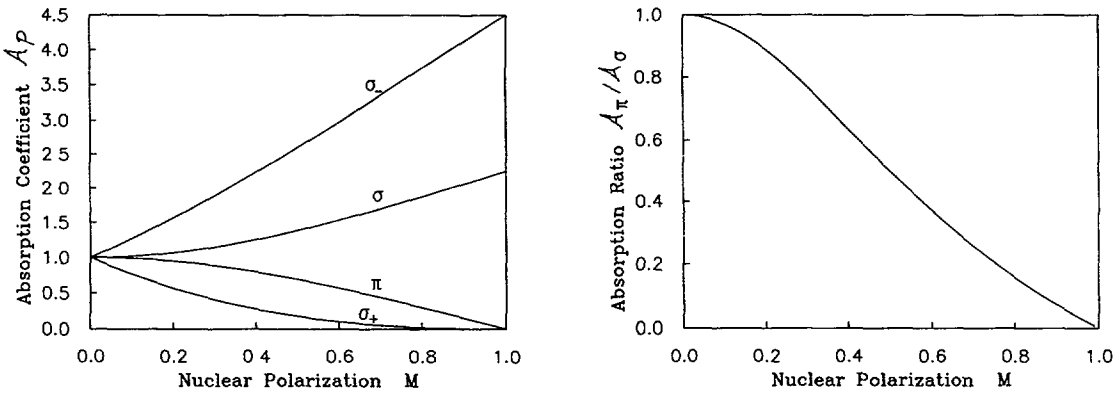


Fig. 2. — a) shows the absorption rate $\mathcal{A}_p$ by the $^3He\ 2\ ^3S_1$ metastables as a function of nuclear polarization $M$ for different polarizations $p$ of the probe beam ($p = \pi$, $\sigma_+$, $\sigma_-$ and $\sigma$ where $\sigma$ is an equal amplitude superposition of $\sigma_-$ and $\sigma_+$). The probe beam is in resonance with the $C_9$ transition. These theoretical results are calculated from reference [16] assuming a constant metastable density $n_m$ for all $M$ and a small fractional absorption. $\mathcal{A}_p$ is normalized to $M = 0$. b) shows the ratio of absorptions for $\sigma$ and $\pi$ polarized light, which is independent of $n_m$.

reference [12], the reason for this is the quadratic dependence of $\mathcal{A}_\sigma$ and $\mathcal{A}_\pi$ on $M$. This dependence is related to the fact that only the *alignement* of the metastable atoms can be detected with $\pi$ and $\sigma$ polarized probes. By contrast, as $M$ increases, the curves $\mathcal{A}_\pi$ and $\mathcal{A}_\sigma$ separate rapidly, making the absorption method based on $\mathcal{A}_\sigma$ and $\mathcal{A}_\pi$ particularly well suited to highly polarized samples. Figure 2b shows the ratio $\mathcal{A}_\pi/\mathcal{A}_\sigma$. We note the sensitivity of the ratio at high $M$ values. The ratio of the measured absorption signals becomes independent of small variations in probe laser intensity as well as variations in the density of metastable atoms. In practice, we measured the normalized absorption ratio

$$[\mathcal{A}_\pi(M)/\mathcal{A}_\pi(M=0)]/[\mathcal{A}_\sigma(M)/\mathcal{A}_\sigma(M=0)]\,.$$

In the earlier absorption experiments of references [3, 11] and [15], the absorption ratio between $\sigma_-$ and $\sigma_+$ probe light was measured. It was then necessary for the probe beam to be coaxial with the pumping beam and the magnetic field. This is because it is the magnetic field which defines the quantization and hence the polarization axis. In earlier work, the probe was not exactly coaxial with the pump light and there was a small angle between the field axis and the probe beam. As a result, what was initially circularly polarized light had a small admixed component of linear polarization when projected onto the quantization axis. From a practical point of view, this measurement is also less desirable because it is experimentally more difficult to generate a probe beam which is purely circularly polarized than a beam which is linearly polarized ; this is simply due to typical imperfections in most quarter wave plates (i.e. a weak ellipticity is hard to avoid). These practical considerations were discussed in reference [12] where the authors measured only $\mathcal{A}_\sigma$. At the time of these experiments lasers were not available and lamp sources were used. As a result, the values of $M$ were smaller and the measurement was significantly less accurate than in the present experiment.

In our experimental geometry, the probe polarizations are created by using a linearly polarized probe which propagates in a direction perpendicular to the quantization axis and for which the axis of polarization is at an angle $\theta \approx 45°$ relative to the quantization axis. When this probe field is projected onto the quantization axis, it decomposes into two linearly polarized field components. One component ($p = \sigma$) has a polarization perpendicular to the quantization axis and is a superposition of equal amounts of circularly polarized light $\sigma_+$ and $\sigma_-$. The other component $\pi$ corresponds to the component with linear polarization along the field axis. This geometry has several important advantages. An error in $\theta$ only changes the relative amplitude between the $\sigma$ and $\pi$ components. Furthermore, the two components of the probe beam are inherently superimposed on the sample, thus eliminating errors due to the spatial distribution of atoms within the discharge. Finally, in our method the absorption of the two probe polarizations is made simultaneously and atoms of the exact same velocity class are compared at the same time in order to form the ratio $\mathcal{A}_\pi/\mathcal{A}_\sigma$.

## 2. Experimental set-up.

Figure 3 shows the experimental set-up which consisted of three distinct parts : the helium cell and optical pumping system, the absorption measuring system and the polarization analysis system for the light emitted by the discharge.

2.1 THE CELL AND THE OPTICAL PUMPING SYSTEM. — The helium cell was a simple right circular cylinder made from pyrex, 5 cm in length and 5 cm in diameter, filled with high purity $^3$He (isotopic purity 99 %) and sealed after baking and filling. The pressure in the cell at the time of seal-off [19] was measured using a baratron pressure gauge to within an accuracy of about 1 %. The 2 $^3S_1$ atoms were populated by an RF discharge induced in the cell by two thin wire electrodes wrapped around the circumference of the cell, one at each end. Most of the

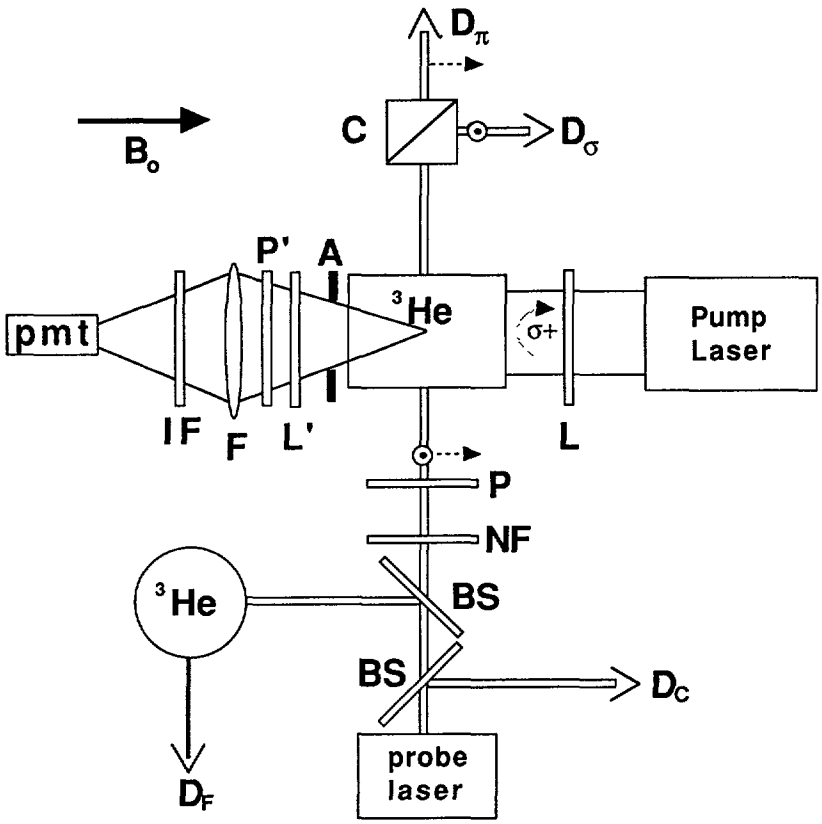


Fig. 3. — Experimental set-up : BS - beam splitter, NF - neutral density filter, P - linear polarizer at 45° from the plane of the figure, C - polarizing beam splitter cube, $D_\pi$, $D_\sigma$, $D_F$ and $D_c$ are Ge detectors for $\lambda = 1.08$ μm, L - $\lambda/4$ plate for $\lambda = 1.08$ μm, A - aperture, L' - rotating $\lambda/4$ plate for $\lambda =$ 668 nm, P' - linear polarizer, F - lens, IF - interference filter for $\lambda = 668$ nm, PMT - photo-multiplier tube, $\mathbf{B}_0$ - applied magnetic field (typically 20 G).

measurements described in this paper were made using a 5.5 MHz discharge frequency. The cell was centered in a static magnetic field $\mathbf{B}_0$ created by a Helmholtz coil pair co-axial with the axis of the cell. Field magnitudes between 5 and 50 G were used. The optical pumping beam propagated along the field axis and was delivered by a continuous lamp pumped LNA laser [4-6]. This laser delivered approximately 3 watts total power in a line width of about 2 GHz. The beam diameter of the pumping beam inside the cell was approximately 3 cm, filling a large fraction of the cell volume. The light emitted by the laser was linearly polarized, and a single quarter wave plate, L, was used to circularly polarize the light before it entered the cell. For pumping cells with pressures of less than 3 torr, the laser was tuned to the $C_8$ transition $\left(2\,^3S_1, F = \frac{1}{2} \rightarrow 2\,^3P_0\right)$ whereas for pressures above 3 torr, pumping on the $C_9$ transition $\left(2\,^3S_1, F = \frac{3}{2} \rightarrow 2\,^3P_0\right)$ was preferred due to the higher attainable values of $M$ for this pumping transition at high pressures [16]. A set of crossed induction-detection NMR coils (not shown in Fig. 13) were installed to monitor the build-up and relaxation times of the polarization. By saturating the NMR transition, we were also able to accurately establish the $M = 0$ state. Pulsed NMR measurements of free induction decay times were used to determine static field gradients, and three first order compensation coils, described elsewhere [20], were

used to reduce field inhomogeneities to less than 0.1 G/m. Additional transverse Helmholtz field coils positioned along the two axes perpendicular to the primary field coils were used in conjunction with a magnetometer to compensate for stray static field components, such as the earth's field, and thus assuring that the applied field was colinear with the pumping axis.

2.2 THE DETECTION SYSTEM OF THE ABSORPTION. — The absorption probe propagated perpendicular to $\mathbf{B}_0$ (see Fig. 3) and was generated by a diode pumped LNA laser [21-23] operated single-mode which was distinct from the pumping laser. A 5 mm length LNA crystal was pumped by a diode array laser which was capable of producing 500 mW at 800 nm and used a focusing arrangement described elsewhere [21]. The LNA laser cavity was about 50 cm long. It included a 10 cm focal length lens and was bounded by a planar mirror of transmissivity 1 %. The crystal was pumped on axis through one end which was polished and coated as a high reflector for 1.08 μm. A birefringent filter placed at the Brewster angle and a coated 0.2 mm thick etalon at near perpendicular incidence were used to tune the laser and to assure single mode operation. This laser produced approximately 10 mW of power at 1.08 μm and was attenuated using neutral density filter NF to approximately 0.1 mW (see Fig. 3) so as to minimize perturbation of metastable level populations. The probe intensity was chosen such that the absorption fraction was linear in probe intensity and such that the measured absorption ratio $\mathcal{A}_\pi/\mathcal{A}_\sigma$ was independent of its value.

Although no active feedback was used on the probe laser, once tuned to the $C_9$ transition the system would remain on resonance for several hours without adjustment. The laser was tuned onto resonance by hopping the cavity modes by tilting the etalon, while simultaneously monitoring the fluorescence light at 1.08 μm emitted by a $^3$He cell illuminated by a small fraction of the beam (see Fig. 3). For frequency scanning, the etalon was mounted on a 5° full deflection angle galvanometric device (galvoplate) taken from a Coherent 699 dye laser. Another beam splitter deflected a small fraction of the probe light which was detected by Ge detector $D_c$ and used as a reference for subtraction circuits placed before the absorption demodulation electronics (commercial phase sensitive detectors or « lock-ins ») ; using this technique we were able to compensate for intensity noise on the absorption signals $\mathcal{A}_\pi$ and $\mathcal{A}_\sigma$. The probe frequency was modulated on and off the $C_9$ resonance by driving the galvoplate at 15 Hz, and the two absorption signals were measured synchronously. In this way we were able to measure absorption due exclusively to metastable atoms in a continuously operating discharge. The amplitude of the frequency modulation was approximately 2 GHz, chosen to assure that the probe was moved completely off the $C_9$ resonance without interacting with the $C_8$ line located 6.6 GHz away. By contrast, the Doppler width of these lines was approximately 0.9 GHz (half width at half maximum). The tuning of the probe laser frequency and the selection of modulation amplitude were continuously monitored by reference to the separate $^3$He fluorescence cell. We verified that changing the amplitude of the modulation by a factor of two was of no consequence for our results. Note that even if the frequency tuning of the laser was not perfectly on resonance, this would not have affected the measurements of the ratio $\mathcal{A}_\pi/\mathcal{A}_\sigma$.

A linear polarizer P was used to set the angle $\theta$ of probe polarization with respect to the quantization axis (an angle of approximately 45°). After passing through the cell, the probe light was split by a polarizing beam splitter cube C, which was oriented to separate polarization components perpendicular to and along the magnetization axis. The individual polarization components were then detected by Ge detectors $D_\sigma$ and $D_\pi$. These signals were analyzed using identical lock-ins, thus yielding signals $\mathcal{A}_\pi$ and $\mathcal{A}_\sigma$. The angle $\theta$ of the polarizer P was adjusted so that the $\mathcal{A}_\pi$ and $\mathcal{A}_\sigma$ values were approximately equal for $M = 0$, this ensured that equal continuous signals were received by the detectors $D_\sigma$ and $D_\pi$, as equal absorption rates were predicted for $\sigma$ and $\pi$ polarizations at $M = 0$ (see Fig. 2a). Preliminary tests were made with

each cell to verify that no fictitious absorption signals were introduced by the glass cell walls, in absence of a discharge.

2.3 THE POLARIZATION ANALYSIS OF THE DISCHARGE LIGHT AT 668 nm. — The light emitted by the helium discharge was observed along the quantization axis parallel to $\mathbf{B}_0$ (see Fig. 3). The light from the central region of the discharge was imaged onto the photocathode of a photomultiplier tube (PMT) using a Fresnel lens F (focal length 10 cm) located at a distance 20 cm from the center of the cell. An interference filter IF selected the helium line at 668 nm. Care was taken to eliminate spurious light reaching the PMT which did not arise directly from the center region of the cell : the side walls of the cell were covered with black tape, the central portion of the apparatus was painted black and a diaphragm, A, 1 cm in diameter, was placed 2 cm behind the plane face of the cell closest to the PMT. Without these precautions the results were found to be as much as 5 % different from the values given here. One possible explanation is that the polarization analyzer should avoid light which passes through the corners of the cylindrical cells, probably slightly birefringent due to sealing. The effective aperture of the lens F could be modified using another diaphragm, thus reducing the solid angle through which light was collected. Decreasing the lens diameter from 9 cm to 3 cm did not cause any change in our measured values. This can be understood if one assumes a $\cos \alpha$ dependence of the polarization of the light beams, as measured at an angle $\alpha$ from the quantization axis ; one calculates that the present detection aperture leads to an average decrease of 1.0 % of the $\mathcal{P}$ signals.

The polarization $\mathcal{P}$ of the light was analyzed on axis using a polarimeter consisting of a quarter wave plate L′ continuously rotating on an air cushion bearing at a frequency $\Omega$, followed by a linear polarizer P′. A phase sensitive detector was then used to measure the rms value $S$ of the signal modulated at frequency 2 $\Omega$. The average value $I$ of the emission line was simultaneously monitored with a DC voltmeter. The amplitude of the polarization rate $\mathcal{P}$ was then given as $\mathcal{P} = \sqrt{2}\, S/I$. The quarter wave plate L′ used for this analysis was a 4 cm diameter antireflection coated quartz plate designed for 668 nm. The linear polarizer P′ was formed from two layers of Polaroid HN32. The imperfections present in this analysis system were measured using the technique described in appendix 2.

## 3. Experimental results.

3.1 EXPERIMENTAL PROCEDURE. — For each cell at a given $^3$He pressure we performed a sequence of operations, yielding a data trace as shown if figure 4. During most of this measurement, the discharge was continuously on. One starts the run with a completely depolarized gas (part 1 in Fig. 4). The polarization of the gas is set to zero using a continuous wave, saturating NMR excitation. The top two traces correspond to absorption signals $\mathcal{A}_\pi$ and $\mathcal{A}_\sigma$ and are approximately equal. The signal $S$ corresponding to the polarization of the 668 nm emission line is also zero. The pumping beam is then turned on, illuminating the cell from one side, and the PMT used for the optical polarization analysis is covered with a non-reflective shutter to protect the photo-cathode and to avoid having depolarized pump light back reflected into the cell. At first $M = 0$ because the saturating magnetic resonance signal remains on (part 2 in Fig. 4). We note that under some experimental conditions there is a small change in the individual absorption signals when the pump laser is applied, but that this change does not affect their ratio. After the NMR signal is turned off, as a function of time, the absorption signal $\mathcal{A}_\sigma$ increases as the polarization $M$ builds up (part 3 in Fig. 4). Simultaneously, $\mathcal{A}_\pi$ decreases. During this period the polarization signal is missing ($S = 0$) because the PMT is blind. The pumping beam is then blocked, and the shutter in front of the PMT is opened. The magnetization $M$ begins to decay with a time constant $T_1$, which depends on the discharge

level, and is typically on the order of 1-2 min. During this time the signal $\mathcal{A}_\sigma$ decreases and $\mathcal{A}_\pi$ increases (part 4 in Fig. 4) whereas the signal $S$ decays. At the end of the run, the polarization $M$ is driven back to zero by using a saturating NMR signal and the signals $S$, $\mathcal{A}_\pi$ and $\mathcal{A}_\sigma$ are restored to their initial values (part 5 in Fig. 4). Part 6 in figure 4 shows all three traces when the discharge is turned off, giving the zero values for the signals $\mathcal{A}_\pi$ and $\mathcal{A}_\sigma$ and the DC background signal for the polarization analysis. Special care was taken to provide a good synchronization between all three traces.

To analyze data as shown in figure 4, several values of $M$ were measured during the relaxation period : we took simultaneous values for $\mathcal{A}_\pi$ and $\mathcal{A}_\sigma$, derived the ratio $\mathcal{A}_\pi/\mathcal{A}_\sigma$, normalized it to its value at $M = 0$, and then used the prediction of figure 2b to determine $M$. This value was then compared to the simultaneous value of $\mathcal{S}$ determined from the signal $S$. We note that parts 1 and 5 in the recorded data give the same amplitude of absorption (with the pump laser off) : this is a check that the discharge levels remained constant during the measurement sequence. Data runs where this requirement was not fulfilled were eliminated. We observed from the signals $\mathcal{A}_\pi$ and $\mathcal{A}_\sigma$ that the metastable densities

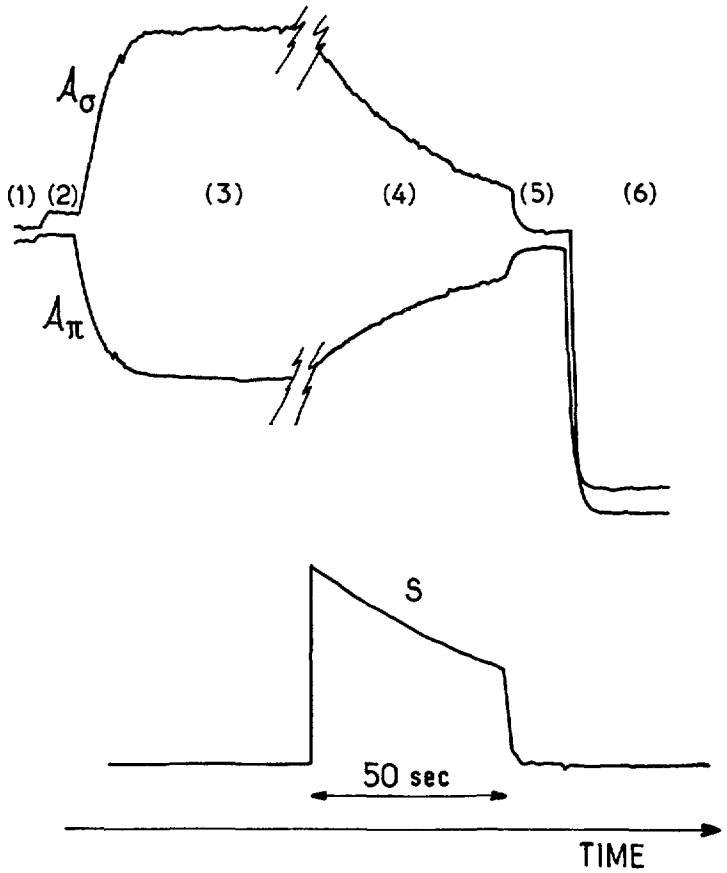


Fig. 4. — $\mathcal{A}_\pi$ and $\mathcal{A}_\sigma$ are absorption signals recorded with the transverse probe beam. $S$ is the demodulated AC signal measured by the PMT for the 668 nm line. (1) Pump laser off, NMR on ($M = 0$). (2) Pump laser on, NMR on ($M = 0$). (3) Pump laser on, NMR off (polarization $M$ builds up). (4) Pump laser off, NMR off ($M$ relaxes). (5) Pump laser off, NMR on ($M = 0$). (6) Discharge off.

$n_m$ for a given discharge level do not remain constant as a function of nuclear polarization. The relative variation of $n_m$ and its sign depend on the cell pressure and can be attributed to several collisional processes showing a polarization dependence. For example in the 0.8 torr cell at a weak discharge level we observed a decrease of $\approx 10$ % of the density $n_m$ as $M$ increased from 0 to 80 %. The relative change was observed to be smaller at higher discharge levels. As noted earlier, these variations do not affect our absorption measurements because of the ratio technique used.

We note that all of the measurements of $M$ and $\mathcal{P}$ were made in the absence of the pump laser beam in order to avoid overpolarization effects in the metastable state which can arise while atoms interact with the laser [16]. However, these effects were very small in any case. This was shown experimentally : there was no discontinuity in the absorption traces between parts 3 and 4 in figure 4 at the moment when the laser was turned off, at full polarization. It was also observed that with the pump laser on, the measured absorption was the same whether the probe beam did or did not cross the pump beam ; this measurement interpreted using the model of reference [16] indicates that the overpolarization effects for the $n_m^*$ fraction of the metastable atoms are less that $10^{-2}$. We use this result and the results of appendix 1 to examine the validity of the simplified model, as discussed in section 1. On the other hand, at $M = 0$ we observe small changes in the metastable density $n_m$ in the presence of the pump laser, as mentioned earlier. Both $\mathcal{A}_\pi$ and $\mathcal{A}_\sigma$ signals vary in the same sense at the discontinuity between parts 1 and 2 in figure 4. This effect, which occurs only when the laser is tuned into resonance with the atomic line, is not yet fully understood. However, we have no reason to believe that these effects could have perturbed the present measurements, taken with the pump laser off and at high $M$ values.

3.2 VARIOUS CHECKS ON THE RESULTS ; DETERMINATION OF ERROR BARS. — Figure 5 shows an example of the results obtained for two cells containing 0.3 and 3.0 torr of pure $^3$He. We have plotted the values of the polarization signals $\mathcal{P}$ at 668 nm *versus* the nuclear polarization $M$ deduced from absorption signals, both measurements being taken at simultaneous times during the decay of the polarization as shown in figure 4 part 4. These results were obtained

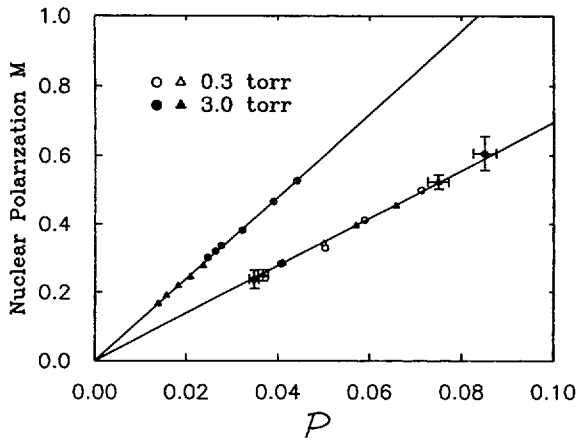


Fig. 5. — Horizontal axis : circular polarization $\mathcal{P}$ of the 668 nm signal. Vertical axis : nuclear polarization $M$ deduced from the absorption signals (see Fig. 4) using the theoretical curve of figure 2b. $^3$He pressures : 0.3 torr and 3.0 torr ; $B_0 = 20$ G. Circles and triangles refer to low and high discharge levels respectively. The straight lines are least squares fits to the data (see text).

using a weak discharge and initial pumping with a 3 watt total power. Note that the values of $M$ in excess of 85 % have been produced in the best cases at low sample pressure and very low discharge level (not shown in this figure). On this figure are shown the experimental error bars ; they arise from the measured signal to noise ratio and include the uncertainty due to the synchronization between the signal on all three traces at any given instant. Little data was taken for $M < 20$ % because of the lack of sensitivity of the absorption technique at low polarizations. Note that the uncertainty in $M$ depends on the discharge level and is smaller when the discharge is bright and the absorption is strong. The straight lines in figure 5 are linear least squares fits to the data constrained to include the $M = 0$ point at the origin. The fits fall well within the error bars, and verify a linear dependence of $\mathcal{P}$ with $M$ over a large range of $M$ values (up to 80 %). In all cases the pessimistic error bars for the straight line fits were less than 1 %. As expected, different slopes are observed for the two pressures : $\mathcal{P}$ signals are reduced at higher pressures due to the collisions in the 3 $^3$D state which partially destroy the electronic orientation before the decay through spontaneous emission. This result was predicted [13] and observed in earlier work [15].

Several measurements were performed to examine the influence of various experimental parameters on the slopes resulting from the straight line fits. Many of these tests were carried out using a cell filled at 0.8 torr for which the signal to noise ratio is rather good for both methods of polarization measurement. Figure 6 shows data obtained with this cell at three different discharge levels, for a fixed excitation frequency of 5.5 MHz ; the three levels correspond to relaxation times $T_1$ ranging from $\approx 30$ to $\approx 300$ s (at 0.8 torr, the value of $I$, the intensity of the continuous signal from the 668 nm line as recorded by the PMT, was approximately 5 times larger at the short $T_1$ than for the long $T_1$ case). Clearly there is no effect of discharge level on the slope of figure 6, within the precision of the measurement. This observation suggests that the polarization of the line at 668 nm is quite insensitive to cascade and collisional effects with ions and electrons generated in the plasma. Similarly the RF frequency of the discharge was varied. Figure 6 also shows data taken with three frequencies : 0.62, 5.5 and 18.1 MHz. No deviation from the slope was observed. Similar data were taken at other pressures. In short, no discharge condition influenced the calibration of the $\mathcal{P}$ signals.

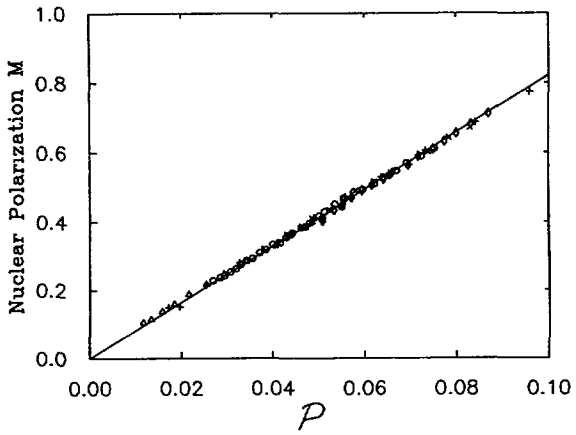


Fig. 6. — Horizontal axis : circular polarization $\mathcal{P}$ of the 668 nm signal. Vertical axis : nuclear polarization $M$ deduced from the absorption signals (see Fig. 4) using the theoretical curve of figure 2b. $^3$He pressure : 0.8 torr, $B_0 = 20$ G. This figure displays results obtained under various discharge conditions : different symbols correspond to different discharge levels and excitation frequencies. The straight line is a least squares fit to all the data points. Since all the data points fall on a single line, the meaning of symbols is not detailed.

Various tests related to the orientation of the applied magnetic field $\mathbf{B}_0$ were also performed. Actually, if $\mathbf{B}_0$ had not been coaxial with the probe beam, then what was thought to be a linearly polarized probe would have had, when projected onto the field axis, both circularly and linearly polarized field components. The effect of such a misalignment would have been to reduce the $M$ values measured by absorption. We described earlier the compensation of the earth field that we used. It turned out to be rather crucial, as without this compensation a 5 % decrease in $M/\mathcal{T}$ values was measured. To further show that this compensation was adequate, we found that, within experimental accuracy, the measured ratio was insensitive to the value of $\mathbf{B}_0$ below 20 G. This observation is consistent with the known weak variation of the ratio with magnetic field (see Sect. 3.3 and Refs. [13] and [14]). Reversal of the absolute direction of $\mathbf{B}_0$ had no effect on our results. Further, changing the sense of circular polarization of the pump light also had no consequence.

Finally, we examined the imperfections of the polarizers and waveplate used to perform the polarization analysis at 668 nm line, imperfections which are likely to reduce the measured values of $\mathcal{T}$. A detailed discussion of the effect of these imperfections is presented in appendix 2, which shows measurements performed with test optics. The analysis takes into account the imperfections in polarization of the polarizer P', the retardation angle between fast and slow axes of the waveplate L', as well as uncertainties in the relative angle between these and the test optics. From this analysis we conclude that our measurements have underestimated $\mathcal{T}$ values by approximately 0.8 % as compared to the values expected in the case of perfect optical components (see appendix 2). Precise values are given in the table I.

From results as shown in figures 5 and 6 we deduced a value for the slope of the straight line fit, as well as confidence levels in this fit, determined from rms scatter in the data about this line, and in most cases, dispersion between successive data runs under otherwise identical conditions. The estimated accuracy of our values for $M/\mathcal{T}$ is about 1.8 % at 0.8 torr where we took a great number of measurements. It is typically of order 2-4 % for pressures between 0.3 and 3.0 torr where the signal to noise ratio for the absorption method is at a maximum. The precision decreases at higher pressures because $\mathcal{T}$ signals are reduced by atomic collisions as discussed earlier and also because the maximum $M$ value achievable is reduced, as discussed for example in references [17] and [24]. The accuracy also decreases at very low pressures because the signal to noise ratio of the absorption signal drops with the absolute number of absorbers.

3.3 RESULTS AT DIFFERENT FIELDS AND PRESSURES. — The polarization $\mathcal{T}$ of the emitted 668 nm line at a given value of $M$ is expected to depend on the magnetic field $\mathbf{B}_0$. This was first investigated in references [13] and [14]. The reason for the decrease is that $\mathcal{T}$ signals originate from the coupling between nuclear and electronic variables in the 3 $^1$D state. At finite magnetic field $\mathbf{B}_0$ there is a partial decoupling of these variables due to the competition between the Zeeman and hyperfine terms in the atomic Hamiltonian. At high fields, $\mathcal{T}$ signals drop to zero, so that the field dependence of these signals can provide a method for evaluating the hyperfine components of the emitting excited atomic levels [13]. The prediction of the field dependence of the $\mathcal{T}$ signals is given by formulas I.B.14 and I.B.30 in reference [13]. For level 3 $^1$D of $^3$He, the computed relative variation is shown in figure 14 of reference [13], which also displays an experimental verification performed by the authors.

Most of our data were taken in a magnetic field of 20 G : this value was found convenient for producing a good colinearity between the applied field and the pumping axis. However, this choice of field values implies a small decrease of the measured $\mathcal{T}$ signals as compared to the zero field limit. From reference [13], this is found to be 1.2 % at 20 G, which is on the order of our experimental error bars. In order to check the field dependence in the present experimental configuration, we varied $\mathbf{B}_0$ between 5.0 and 50 G. Results are shown in figure 7. These results

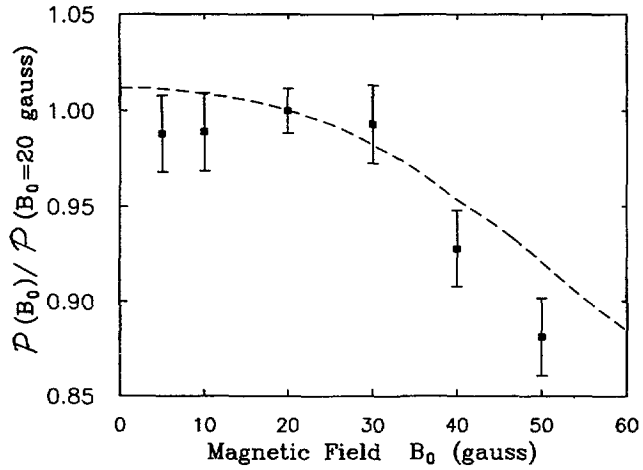


Fig. 7. — Horizontal axis : static magnetic field $B_0$ in gauss. Vertical axis : value of the ratio $\mathcal{S}/M$ deduced from the slopes of the straight line fits as shown in figures 5 and 6. $M$ is the nuclear polarization, $\mathcal{P}$ is the polarization rate of the 668 nm line. The squares are the present experimental results normalized to the result obtained at 20 G and the dashed curve is the theoretical result from reference [13].

were normalized to the value obtained at 20 G where most of the data were taken. The dashed line corresponds to the theory of reference [13]. We find a reasonable agreement with this theory.

The pressure dependence of $\mathcal{S}$ signals was investigated between 0.15 and 6.45 torr, corresponding to the experimentally effective range for optical pumping. $M$ values which can be achieved are strongly limited below 0.15 torr by the relaxation of the 2 $^3S_1$ metastables by diffusion to the cell walls and for pressures much above a few torr by the relative drop in the metastable density [17, 24]. Figure 8 displays the measured $\mathcal{S}/M$ ratio as a function of the

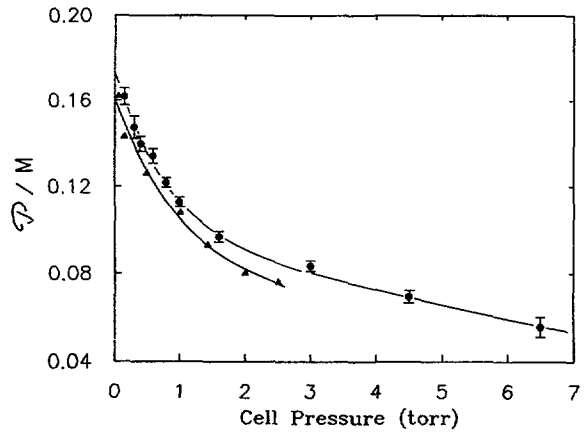


Fig. 8. — Horizontal axis : $^3$He pressure in torr. Vertical axis : measured ratio $\mathcal{S}/M$. These values correspond to column (3) in the table I ($M$ values derived from the model of Ref. [16]). Circles are this experiment (error bars are discussed in the text), triangles are data of reference [15]. Solid lines are guides to the eye.

sample pressure. In fact, these numbers are taken directly from the least square fits corrected at low pressure according to appendix 1 ; the estimated error bars, as discussed in the previous section, increase at both low and high pressures. Note that the results shown in figure 8 are directly derived from this experiment, performed at 20 G, in a given geometry, and with imperfect polarizing optics.

Table I summarizes the results of the present work. It displays the measured values of the $M/\mathcal{S}$ ratios for different sample pressures. Column (2) gives the results derived directly from the present experiment. Column (3) incorporates the corrections estimated in appendix 1 which result from a more elaborate model. Column (4) gives the corresponding values to be expected in more ideal conditions, namely i) using perfect optics in the polarization analyzer for the 668 nm line and ii) with a very small solid angle for the collection of the 668 nm line. Column (5) adjusts the values of column (4) for the case of zero magnetic field. As already discussed, effects (i), (ii) and finite magnetic field decrease $\mathcal{S}$ signals as compared to the present situation. Ideally, $M/\mathcal{S}$ is to be corrected down by factors of 0.8, 1.0 and 1.2 % respectively for each of the three effects in turn, altogether a 3.0 % total correction.

## 4. Discussion.

Now consider figure 8 which summarizes our work. The present results fall consistently above the previous work of Pinard *et al.* [15], for which there were no available error bars. The

Table I. — *Measured values of* $M/\mathcal{S}$ *as a function of the* $^3$He *pressure in torr. M is the nuclear polarization derived from optical absorption measurements.* $\mathcal{S}$ *is the degree of circular polarization of the* 668 nm *line. Column* (2) *gives the values as measured for* $B_0 =$ 20 G *using a simplified optical pumping model (see text). The other columns include successive corrections. Column* (3) *includes corrections of column* (2) *at low pressures* ($p < 0.8$ torr) *which account for the relaxation of the metastable atoms. Column* (4) *includes further corrections for various experimental imperfections :* $M/\mathcal{S}$ *is thus reduced by* 0.8 % *for imperfections in the polarimeter optical components and by* 1.0 % *for finite solid angle in the detection. Column* (5) *includes the* 1.2 % *decrease of* $M/\mathcal{S}$ *correcting the values of column* (4) *to* $B_0 = 0$ *(theoretical correction, see text).*

| (1) | (2) | (3) | (4) | (5) |
|---|---|---|---|---|
| $^3$He pressure (torr) | simplified model | complete model | perfect optics | zero field |
| 0.15 | 6.06 ± 0.15 | 6.18 | 6.07 | 6.00 |
| 0.30 | 6.75 ± 0.24 | 6.78 | 6.66 | 6.58 |
| 0.40 | 7.14 ± 0.18 | 7.16 | 7.03 | 6.95 |
| 0.60 | 7.46 ± 0.19 | 7.47 | 7.28 | 7.25 |
| 0.80 | 8.21 ± 0.14 | 8.21 | 8.06 | 7.96 |
| 1.0 | 8.86 ± 0.17 | 8.86 | 8.70 | 8.59 |
| 1.6 | 10.33 ± 0.27 | 10.33 | 10.14 | 10.02 |
| 3.0 | 12.0 ± 0.35 | 12.0 | 11.76 | 11.62 |
| 4.5 | 14.5 ± 0.61 | 14.5 | 14.2 | 14.0 |
| 6.5 | 18.0 ± 1.5 | 18.0 | 17.7 | 17.5 |

absolute discrepancy is of order 10 % and is not surprising : the earlier work had been carried out not as an accurate calibration of the method, but more as a demonstration of its efficiency. We have already discussed the uncertainties of reference [15] due to the use of lamps as sources for the absorption probe beam, whose coincidence with the atomic absorption line is ambiguous. We think that the use of a single frequency laser was a substantial improvement of the present work, as well as the perpendicular geometry of the absorption probe beam. More care was also taken in the present work to select good optical components for the optical analysis and, by far, more tests for systematic error were performed. In short, we believe that the present results are significantly more reliable than previously published ones as a direct calibration of the polarization method.

It would be interesting to compare the present results to those obtained from other laboratories using other methods, as the systematic errors intrinsic to other methods will be different. Researchers at Caltech [10] are currently pursuing absolute measurements of nuclear polarization determined from NMR, using calibration to a cell containing pure water as a reference. These results will be reported soon. Early communication regarding this work indicates good agreement, in particular at pressures above 1 torr.

Comparing the two methods used here to measure the nuclear polarization, it is clear that monitoring the polarization distribution of the 668 nm fluorescence line is the easiest technique, given that is does not require a probe laser. For this reason, we present our results as a calibration of that method, to be used for example in future measurements with polarized beams and targets for nuclear and high energy physics. We note that several groups have initiated major research programs to attain high density polarized $^3$He samples for external targets. In these efforts, the increase in density relies either on cooling [25] or on mechanical compression [26, 27].

In conclusion we want to stress the point that if the present numbers are to be used under different experimental conditions than ours, much care must be taken to correctly interpret the data. In particular the imperfections of the polarization analyzers must be measured seperately, if one wants to fully benefit from the accuracy found in the present work.

**Acknowledgements.**

The authors thank Jean Brossel for careful preparation of the Helium cells used in this work and Christian Larat for the computer program described in appendix 2. We are grateful to Tom Gentile of the California Institute of Technology for early communication of NMR results and to Christian Larat, Tom Gentile and A. Aspect for discussions regarding the correction described in appendix 2. We are also grateful to Christian Deverdun of Coherent Scientific, France for his kind loan of the galvoplate etalon assembly used in the LNA probe laser.

## Appendix 1

### Approximations of the optical pumping model : validity and corrections.

In this article, we derived the nuclear polarization $M$ of the 1 $^1S_0$ ground state atoms of $^3$He from measurements of polarized light absorbed by 2 $^3S_1$ metastable atoms. As discussed in section 1, this method relies on a model for the kinetics of the $^3$He optical pumping mechanism. A simplified model was used leading to a unique curve relating the ratio $\mathcal{A}_\pi/\mathcal{A}_\sigma$ to $M$ (see Fig. 2b) independent of other physical parameter such as pressure or discharge conditions. The approximation consists of assuming that the metastability exchange collisions with the ground state atoms are the dominant process ruling the evolution of the metastable populations, thus neglecting the relaxation processes in the 2 $^3S_1$ metastable state and various effects due to the pumping light. We evaluate here the resulting error for the

determination of $M$ by comparing the predictions of this simplified model with the predictions of the more complete model of reference [16].

Let us note that because our calibration measurements were performed with the pump laser off, the value of $n_m^*/n_m$ is not required (see Ref. [16]). On the other hand, the value of $\tau_r$, the metastable relaxation time, is needed. In the model of reference [16] the various processes responsible for the relaxation of the metastable state orientation (collisions with the walls, collisions in the gas phase etc.) are phenomenologically described by a unique relaxation time $\tau_r$. Note that the relaxation time is not necessarily an average property of the metastable atoms in the cell, because of the deexcitation of the atoms when they hit the walls. Thus, $\tau_r$ can depend on the details of the experimental geometry and on the position of the discharge electrodes, as the atoms are created with increasing probability near the electrodes. In this work, the relevant $\tau_r$ value is the mean metastable relaxation time for atoms detected along the path of the narrow transverse probe beam and has not been precisely determined experimentally. Actually it is likely to slightly differ from the $\tau_r$ time used in reference [16], where an average time over the cell volume was considered. In reference [16] one considered as a possible $\tau_r$ value the mean time $\tau_d$ for a metastable atom to diffuse to the cell walls. Another estimate of a lower bound for $\tau_r$ was derived from the measured ground state relaxation time $T_1$, which includes a contribution from the metastable relaxation through exchange collisions [16]. For instance in a cylindrical cell 5 cm in length and 5 cm in diameter at 0.15 torr of pressure, $\tau_d = 0.225$ ms, whereas a lower bound for $\tau_r$ is 0.19 ms when $T_1 = 25$ s and $n_m/N = 2 \times 10^{-6}$ (as measured in the present experiment) : thus $\tau_r = 0.2$ ms is a sensible estimate of the average relaxation time $\tau_r$ in the cell. One can also assume that such a value is a reasonable estimate of the relevant parameter for the calculation of the present absorption signals. This value of $\tau_r$ can be compared with $\tau_e$, the average time between two metastability exchange collisions. $\tau_e$ increases linearly with $1/p$ (where $p$ is the helium pressure) whereas $\tau_r$ varies roughly linearly with $p$ as does $\tau_d$. Thus the ratio $\tau_r/\tau_e$ is expected to vary like $p^2$ and hence the simplified model should hold best a high pressure (where $\tau_r \gg \tau_e$). In the previous example $\tau_d/\tau_e \sim 2 \times 10^2$ at 0.15 torr (the lowest pressure considered here) but $\tau_d/\tau_e \sim 5 \times 10^3$ at 0.8 torr (a pressure at which most of our experimental checks were performed).

From this one computes the more exact value of $M$, which is found slightly higher than that derived from the simple model used in this article. The relative error on $M$ is nearly independent of $M$, and equal to 2.0 % at 0.15 torr (assuming $\tau_r = 0.2$ ms). At higher pressures $p$ the error is expected to decrease as $1/p^2$. In table I column (3) the $M/\mathfrak{F}$ values have been corrected up for the measurements at $p \leq 0.6$ torr. At higher pressures, the correction becomes too small to change the presented values.

Finally let us mention that there are possibilities to reduce this error on the calibration of $M$ resulting from the imprecisely known relaxation rate of the metastable atoms. It could be needed if the present method were applied to even lower pressures, or if experimental improvements were decreased substantially all the other uncertainties. First one could develop an experimental procedure to actually measure the relevent value of $\tau_r$, based on the observation of transient signals when the discharge is interrupted. Second one could find experimental conditions to minimize the metastable relaxation : for instance one could use a larger cell to decrease the destruction rate of metastable atoms by collision with the walls ; one could also pulse the discharge and perform the measurement in the afterglow : the absorption signal would decrease proportional to the metastable density, but on the other hand one would avoid the creation of unpolarized metastable atoms by the discharge excitation and all the relaxation processes occuring in the plasma, such as collisions with other excited species, would be suppressed.

## Appendix 2

### Measurement of the optical imperfections of the polarimeter.

Figure 9a shows the optical arrangement used to detect the circular polarization of the light emitted by the discharge : quarter wave plate L′ rotates at frequency $\Omega$, P′ is a linear polarizer and the light detected by photomultiplier PMT is modulated at 2 $\Omega$. We define $\phi$ as the phase retardation angle between the two crossed polarizations introduced by L′, and $\varepsilon$ as the amount of opposite polarization transmitted by P′. In the case of ideal optics, $\phi = 90°$ and $\varepsilon = 0$. For perfectly circularly polarized light incident on this system, the transmitted intensity would be modulated at a frequency 2 $\Omega$ with 100 % modulation amplitude. For $\phi \neq 90°$ and $\varepsilon \neq 0$ the modulation amplitude is smaller, causing an underestimation of $\mathcal{P}$. To evaluate $\phi$ and $\varepsilon$ we performed two measurements using a second linear polarizer (P″) and quarter waveplate (L″), identical to P′ and L′ respectively.

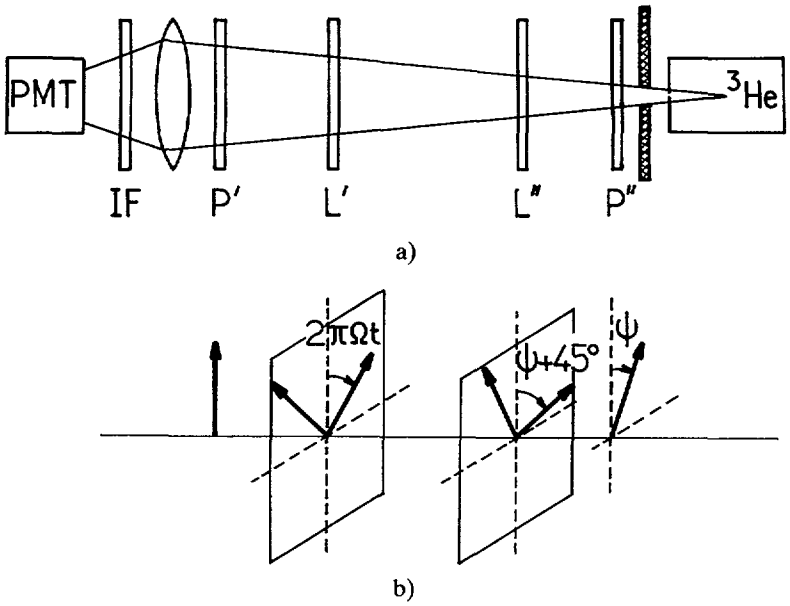


Fig. 9. — Measurement of the optical imperfections of the polarimeter shown in figure 3. a) Experimental configuration using the light emitted at 668 nm by the $^3$He cell and detected using photomultiplier PMT through an interference filter IF. P′ and L′ are the polarizer and the quaterwave plate used in the polarimeter. P″ is another polarizer identical to P′ and L″ is another waveplate identical to P′. b) Polarization vector of the light. $\psi$ is the angle between the axes of P′ and P″. Waveplate L′ rotates at angular frequency $\Omega$.

To interpret our calibrations we introduce an analysis based on the work of Larat [17]. The light polarization is represented by a 2 × 2 matrix $\Pi$, which becomes $\mathcal{M}\Pi\mathcal{M}^+$ after crossing an anisotropical element represented by the matrix $\mathcal{M}$. The advantage of this formalism is that the polarization of the light, as it propagates through successive optical elements, is described as a series of matrix multiplications [13, 28]. For an imperfect polarizer P,

$$\mathcal{M}_P = \begin{pmatrix} 1 & 0 \\ 0 & \varepsilon \end{pmatrix}$$

whereas for a non-absorbing birefringent quarter wave plate L with a retardation angle $\phi$,

$$\mathcal{M}_L = \begin{pmatrix} 1 & 0 \\ 0 & e^{i\phi} \end{pmatrix}.$$

If these elements are rotated in their plane by an angle $\alpha$, then $\mathcal{M}$ transforms into $\mathcal{M}' = \mathcal{S}_\alpha^{-1}\,\mathcal{M}\mathcal{S}_\alpha$, where

$$\mathcal{S}_\alpha = \begin{pmatrix} \cos\alpha & \sin\alpha \\ -\sin\alpha & \cos\alpha \end{pmatrix}.$$

MEASUREMENT 1. — The light crosses P″ and L″, rotating L′ and P′ (see Fig. 9a). The position of L″ is adjusted for the neutral lines at 45° from the axis of P″. The adjustment is made by inserting L″ between crossed polarizers P′ and P″. Let us call $\varepsilon'$ the error in positioning of L″. One turns, in its plane, the circular polarizer consisting of L″ and P″ : both optical elements are rotated simultaneously at an angle $\psi$, $\psi$ being the angle between P′ and P″ (see Fig. 9b). If the components were ideal, the modulation at 2 $\Omega$ should have an amplitude of exactly 100 %. For imperfect elements, the modulation amplitude can be both greater or less than this value. In figure 10 we show the results for our optics. The amplitude of the modulation varies with $\psi$ between 95 and 104 % with the expected periodicity of 180°. The size of this variation with $\psi$ is rather sensitive to the initial positioning of L″ with respect to P″, set in a self consistent manner to minimize this variation. The oscillations in figure 10 are then fit with the polarization matrix formalism.

If $\Pi_0$ corresponds to the non-polarized light incident on the polarizer P″, then the polarization after crossing P″ and L″, L′ and P′ is given by

$$\Pi_S = \mathcal{M}_{P'}\,\mathcal{M}_{L'}\,\mathcal{M}_{L''}\,\mathcal{M}_{P''}\,\Pi_0\,\mathcal{M}_{P''}^{+}\,M_{P''}^{+}\,\mathcal{M}_{P'}^{+}\,\mathcal{M}_{P'}^{+},$$

with

$$\mathcal{M}_P' = \begin{pmatrix} 1 & 0 \\ 0 & \varepsilon \end{pmatrix}$$

$$\mathcal{M}_P'' = \mathcal{S}_\psi^{-1}\begin{pmatrix} 1 & 0 \\ 0 & \varepsilon \end{pmatrix}\mathcal{S}_\psi$$

$$\mathcal{M}_L' = \mathcal{S}_{\Omega t}^{-1}\begin{pmatrix} 1 & 0 \\ 0 & e^{i\phi} \end{pmatrix}\mathcal{S}_{\Omega t}$$

$$\mathcal{M}_L'' = \mathcal{S}_{\psi+\varepsilon'}^{-1}\begin{pmatrix} 1 & 0 \\ 0 & e^{i\phi} \end{pmatrix}\mathcal{S}_{\psi+\varepsilon'}.$$

The trace of matrix $\Pi_S$ contains a term modulated at frequency 2 $\Omega$ whose dependence on $\psi$ has to be fit to figure 10 with the three unknown parameters $\phi$, $\varepsilon$ and $\varepsilon'$. The value of $\varepsilon$ can be determined in an independent experiment : when P′ is a simple plastic HN32 polarizer one measures $\varepsilon = 5 \times 10^{-2}$ ; when the polarizer is doubled we assume $\varepsilon = 0.25 \times 10^{-2}$. We found an experimental uncertainty for the relative angular positioning between P″ and L″ to be less than 2°, hence $\varepsilon' < 2°$. Adjusting the parameters $\varepsilon'$ and $\phi$ we found a best fit for the data of figure 10 using $\phi = 86°$ and $\varepsilon' = 1.5°$. Figure 10 shows also the results calculated with the same values of $\varepsilon$ and $\varepsilon'$ for quarter wave plates of different quality ($\phi = 80°$ and 90°). We thus deduce that $\phi = 86 \pm 2°$ for the present experiment. To illustrate the influence of $\varepsilon$, which might be different for a different experimental set-up, we display in figure 11a the calculated results for $\phi = 86°$, $\varepsilon' = 1.5°$ and $\varepsilon$ ranging from 0 to 0.05. Figure 11b shows the dependence on $\varepsilon'$. The large difference in the oscillation amplitude when $\varepsilon'$ increases indicates that these measurements require careful experimental positioning of elements L″ and P″ to provide a reliable value for $\phi$.

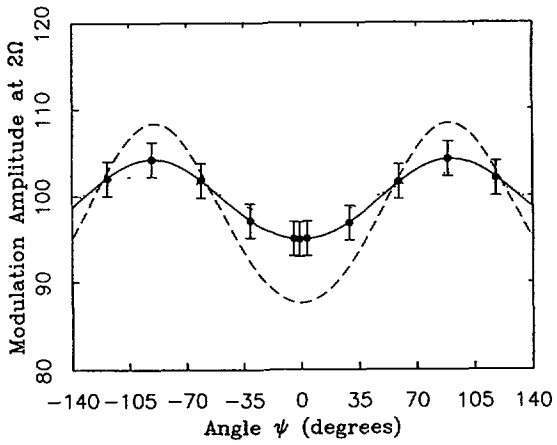


Fig. 10. — Relative amplitude (in percent) of the modulation at 2 $\Omega$ recorded by photomultiplier PMT as a function of angle $\psi$ with the set-up shown in figure 9. The solid line is a fit to the data using $\phi = 86°$ (retardation angle of L'), $\varepsilon = 0.25 \times 10^{-2}$ (extinction coefficient of P') and $\varepsilon' = 1.5°$ (the angular error in the relative positioning of P" and L"). Dotted line : calculated signal for $\phi = 90°$, $\varepsilon = 0.25 \times 10^{-2}$ and $\varepsilon' = 1.5°$. Dashed line : calculated signal for $\phi = 80°$, $\varepsilon = 0.25 \times 10^{-2}$ and $\varepsilon' = 1.5°$.

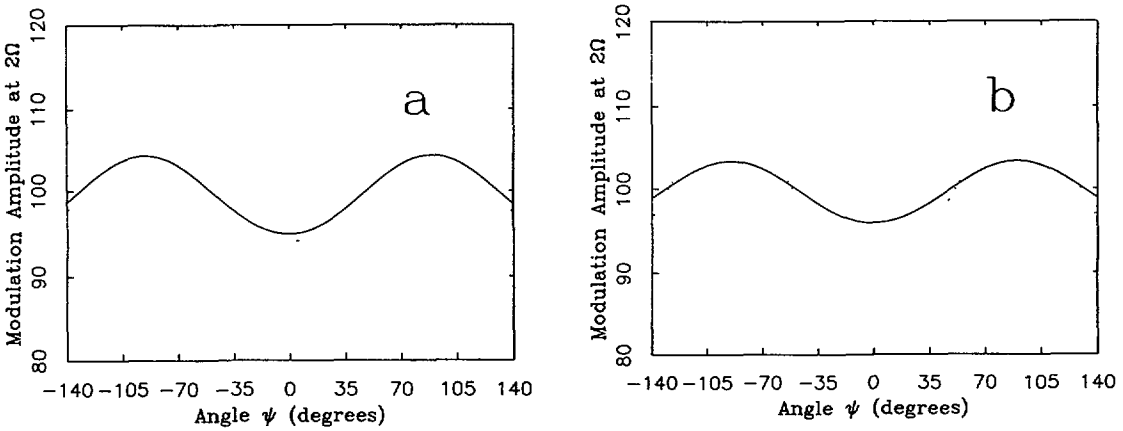


Fig. 11. — Signal modulated at 2 $\Omega$ as shown in figure 10 calculated for different values of the parameters. a) $\phi = 86°$, $\varepsilon' = 1.5°$ and $\varepsilon = 0$ (solid line) and $\varepsilon = 5.0 \times 10^{-2}$ (dashed line). b) $\phi = 86°$, $\varepsilon = 0.25 \times 10^{-2}$ and $\varepsilon' = 0°$ (solid line) and $\varepsilon' = 5°$ (dashed line).

MEASUREMENT 2. — Waveplate L" is then removed. The transmitted light is thus modulated at 4 $\Omega$ since each time a neutral line of L' coincides with an axis of P' there is no phase retardation (see Fig. 9). One then varies the angle $\psi$ between the axis of P" and P' by rotating P". For each value of $\psi$ one measures the DC average optical signal detected by the PMT as well as the amplitude of the 4 $\Omega$ signal using a lock-in amplifier. The relative amplitude of the 4 $\Omega$ signal for our components is shown in figure 12. Theoretical values of these signals can be computed for arbitrary choices of $\phi$ and $\varepsilon$. Notice that the fit is less sensitive to the parameters than in the case of measurement 1. The dashed line in figure 12 corresponds to ideal elements and the solid line uses the same values $\phi = 86°$ and

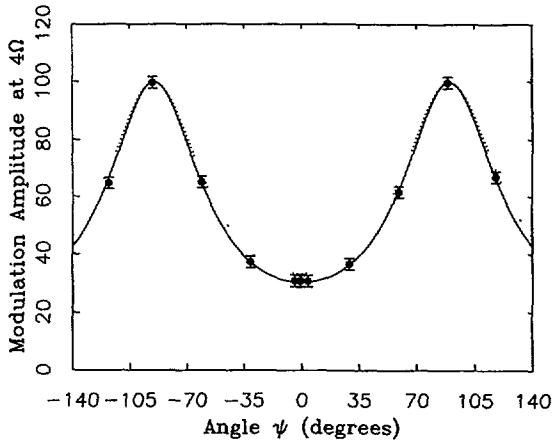


Fig. 12. — Signal detected by PMT as a function of the angle $\psi$ for the measurement of figure 9 when L″ is removed. Circles are modulation amplitude of signal at 4 $\Omega$. Dotted line : results if components were perfect. Solid line : fit to data with $\phi = 86°$ (retardation angle of L′) and $\varepsilon = 0.25 \times 10^{-2}$ (extinction coefficient of P′).

$\varepsilon = 0.25 \times 10^{-2}$ as found from measurement 1. The agreement is satisfactory and confirms the choice of parameters.

Knowing the imperfections of the circular analyzer in the $\mathcal{T}$ measurement, one can thus calculate, using the formalism of the polarization matrices, the amplitude $\mathcal{T}_{max}$ of the modulation at 2 $\Omega$ which one would detect if the light were 100 % circularly polarized. We find that for our evaluated values of $\phi$ and $\varepsilon$, $\mathcal{T}_{max} = 99.2$ %. Hence the values for $\mathcal{T}$ determined in this paper should be increased by 0.8 % to give the values expected in the case of perfect optical components.

## References

[1] Spin Polarized Quantum Systems, S. Stringari Ed. (World Sci. Pub. Co., 1989).

[2] 7th International Conference on Polarization Phenomena in Nuclear Physics (Paris), *J. Phys. Colloq. France* **51** (1990) C6.

[3] COLGEROVE F. D., SCHEARER L. D. and WALTERS G. K., *Phys. Rev.* **132** (1963) 2561.

[4] AMINOFF C. G., LARAT C., LEDUC M. and LALOE F., *Rev. Phys. Appl.* **24** (1989) 827.

[5] PADETHA TIN and SCHEARER L. D., *J. Appl. Phys.* **68** (1990) 950.

[6] AMINOFF C. G., ESSABAA S., BRISSAUD I. and ARIANER J., *Opt. Commun.* **86** (1991) 99.

[7] Polarized $^3$He Beams and Targets, R. W. Dunford and F. P. Calaprice Eds., AIP Conference Proceedings n° 131 (1985).

[8] COHEN-TANNOUDJI C., DUPONT-ROC J., HAROCHE S. and LALOE F., *Rev. Phys. Appl.* **5** (1970) 95 and 102.

[9] CHUPP T. E., WAGSHUL M. E., COULTER K. P., MCDONALD A. B. and HAPPER W., *Phys. Rev. C* **36** (1987) 2244.

[10] GENTILE T., personal communication ;
LORENZON W., GENTILE T. R., GAO H. and MCKEOWN R. D., to be published *Phys. Rev. A.*

[11] GREENHOW R. C., *Phys. Rev.* **136** (1964) A660.

[12] DANIELS J. M. and TIMSIT R. S., *Can. J. Phys.* **49** (1971) 539 ;
TIMSIT R. S. and DANIELS J. M., *Can. J. Phys.* **49** (1971) 545.

[13] PAVLOVIC M. and LALOË F., *J. Phys. France* **31** (1970) 173.
[14] LALOE F., Thèse d'état (Paris), *Ann. Phys. France* **6** (1971) 5.
[15] PINARD M. and VAN DER LINDE J., *Can. J. Phys.* **52** (1974) 1615.
[16] NACHER P. J. and LEDUC M., *J. Phys. France* **46** (1985) 2057.
[17] LARAT C., thèse de doctorat de l'Université de Paris VI (1991).
[18] DUPONT-ROC J., LEDUC M. and LALOE F., *Phys. Rev. Lett.* **27** (1971) 467.
[19] It has been noticed by T. Gentile and coworkers that the helium pressure may tend to drop somehow some time after a discharge has been started. This process, which seems to be reversible but not very reproducible, is likely to decrease the low pressure values quoted here by a few percent. However, our calibration method is not affected by the errors in the pressure, in contrast with the method used in reference [10].
[20] HIMBERT M., thèse de docteur d'état (Paris, 1987) p. 42.
[21] AUBERT J. J., WYON C., CASSIMI A., HARDY V. and HAMEL J., *Opt. Commun.* **69** (1989) 299.
[22] BOHLER C. L., *J. Appl. Phys.* **66** (1989) 4614.
[23] CHUANG T. and METCALF H. J., *Appl. Opt.* **30** (1991) 2495.
[24] NACHER P. J., LEDUC M., TRÉNEC G. and LALOE F., *J. Phys. Lett.* **43** (1982) L525.
[25] MILNER R. G., MCKEOWN R. D. and WOODWARD C. E., *Nucl. Instr. Methods* **A 274** (1988) 56.
[26] OTTEN E. W., *Prog. Particle Nucl. Phys.* **24** (1990) 103.
[27] ECKERT G. *et al.*, submitted to *Nucl. Instr. Methods.*
[28] See for instance, BORN M. and WOLF E., Principles of Optics (Pergamon Press, 1969) p. 541 or LANDAU L. and LIFCHITZ E., Théorie du Champ (ed. de la Paix, Moscou, 1964) p. 163.